ILASS-Europe 2002 *Zaragoza 9-11 September 2002*

ADVANCED MODELING OF DROPLET DEFORMATION AND BREAKUP FOR CFD ANALYSIS OF MIXTURE PREPARATION

Roland Schmehl
roland.schmehl@esa.int
Aerothermodynamics Section TOS-MPA, European Space & Technology Centre, The Netherlands

Abstract
The study presents analytical approaches to modeling droplet deformation and breakup by aerodynamic forces at moderate relative velocities. Linear Normal Mode Analysis is used to accurately predict the small-amplitude shape response of a droplet to an aerodynamic surface pressure distribution. To account for variable relative flow conditions, 46 pressure distributions on spheres are correlated to cover the complete range of subcritical Reynolds numbers. Large distortions and shape oscillations are described by a nonlinear analysis considering only a spheroidal mode of deformation. Both concepts provide kinetic equations for deformation parameters, which are suitable for numerical integration within Lagrangian droplet tracking schemes. The effect of droplet motion is taken into account by means of a deformation-dependent drag force model. The stability limit is specified as a critical degree of deformation and is choosen to reproduce experimental data. Irreversible deformation in the breakup phase and fragment characteristics are not considered in the present paper. To systematically validate the different models, they are assessed within a matrix of test case computations ranging from free shape oscillations to deformation of free falling droplets and distortion, propagation and breakup in shock wave and nozzle flows.

Nomenclature

Symbols

c_D	-	Aerodynamic drag coefficient
C_n	-	Pressure coefficient, mode n
D	m	Droplet diameter
E	-	Aspect ratio of droplet
On	-	Ohnesorge number
p	N/m^2	Pressure
P_n	-	Legendre-Polynomial of order n
r	m	Position, droplet reference frame
R	m	Droplet radius, undeformed
Re	-	Reynolds number, flow around droplet
Re_{def}	-	Reynolds number, flow in droplet
t	s	Time
T	-	Nondimensional time
u	m/s	Velocity, inertial reference frame
v	m/s	Velocity, droplet reference frame
We	-	Weber number
y	-	Nondimensional equator coordinate
α	-	Displacement of stagnation point
α_n	-	Displacement time-function, mode n
μ	Ns/m^2	Dynamic viscosity
ϕ	rad	Polar angle
Φ_μ	$N/(m^2 s)$	Dissipation function
ρ	kg/m^3	Density
σ	N/m	Surface tension
ω	-	Nondimensional angular frequency

Indices

$*$	Characteristic value
0	Initial/undeformed value
c	Critical value
d	Droplet/liquid value
n	Order of deformation mode
s	Surface value
∞	Value far from droplet surface

Introduction

Deformation and breakup of liquid droplets by aerodynamic forces are typical phenomena in many multiphase flow processes. An important technical application is mixture preparation in liquid-fueled gas turbines, jet-engines, rocket motors and IC-engines. Modern low-emission combustion concepts often employ some level of secondary droplet atomization in order to generate a well dispersed and fine fuel spray with good evaporation characteristics. In solid rocket motors on the other hand, the phenomena can occur with liquid slag droplets in the accelerating nozzle flow, thus affecting slag deposition in the nozzle region and other operational parameters. Overall, droplet deformation and particularly breakup have a strong impact on the dispersion characteristics and structure of multiphase flows by increasing the flow resistance of the droplets and reducing their sizes.

At moderate relative velocities the fundamental mechanism is a distortion of the droplet by the inhomogeneous pressure distribution on the droplet surface, caused by the external flow. Exceeding a critical intensity, the pressure gradient from stagnation points to droplet equator eventually leads to an irreversible expansion flow resulting in the typical bag breakup phenomena. Non-dimensional parameters characterizing this mechanism are the Weber number We, specifying the intensity of aerodynamic forces relative to the stabilizing surface tension forces and the Ohnesorge number On, quantifying the effect of internal viscous forces

$$\mathrm{We} = \frac{\rho v_{rel}^2 D_0}{\sigma}\ , \qquad \mathrm{On} = \frac{\mu_d}{\sqrt{\rho_d D_0 \sigma}}\ , \qquad \mathrm{Re}_{def} = \frac{v_{rel} D_0}{\mu_d}\sqrt{\rho\,\rho_d}\ , \qquad t^* = \sqrt{\frac{\rho_d}{\rho}}\frac{D_0}{v_{rel}}\ . \tag{1}$$

The Reynolds number $\mathrm{Re}_{def} = \sqrt{\mathrm{We}}/\mathrm{On}$ describes the ratio of inertia forces to viscosity forces in the deformation flow. The characteristic time t^* is a measure for the temporal evolution of the process.

It has further been observed that the deformation response depends not only on the relative intensity of the aerodynamic forces, but also *how* they are applied to the droplet. Limiting cases are the quasi-steady deformation resulting from a slow, gradual loading—e.g. a rain droplet accelerating in free fall—in contrast to the highly dynamic deformation response to sudden shock loading—e.g. a rain droplet captured by a shock front generated by fast moving aircraft. *Slow* and *sudden* are referring both to the characteristic time t^* of deformation. The effect of different loading scenarios is reflected in the value of the critical Weber number, which is $\mathrm{We}_c = 20$ (instantaneous value) for gradual and $\mathrm{We}_c = 13$ (initial value) for sudden loading and negligible viscosity effects [6]. For the latter scenario, distinctive mechanisms of breakup are observed for increasing values of We_0: At $\mathrm{We}_0 = 18$ plume breakup and from $\mathrm{We}_0 = 40$–80 a gradual transition to shear breakup, a mechanism which is often described as a detachment of a liquid boundary layer from the droplet equator [6, 1].

In most practical applications the loading scenario is more complex. Flow fields can be highly inhomogeneous and transient, characterized by turbulence and by large-scale spatial and temporal mean flow variations. Droplet movement in the flow makes the situation even more complicated. Although on a local scale the flow approaching the droplet may still be regarded as uniform, the flow conditions continuously change depending on the time and length scales involved. Thus, to model deformation and breakup within CFD analysis of practical flow fields, these external factors have to be accounted for in addition to the deformation behavior.

Correlations of experimental data are available for specific configurations, e.g. sudden aerodynamic loading in shock tubes or wind tunnels [6, 1], gradual loading along nozzle flow and weakly turbulent flows as well as loading with specific velocity gradients. Due to the time and length scales implied in these experiments, special care has to be taken when selecting the resulting correlations in a general flow field analysis. Nevertheless, once checked for applicability, correlations are efficient and robust and have been extensively used in the past [15]. More versatile in this respect, is the Taylor-Analogy-Breakup (TAB) model. It has been introduced in the frame of CFD analysis by O'Rourke and Amsden [11]. In this model, the droplet is idealized as a dynamical spring-mass-damper system described in terms of a single deformation coordinate. The resulting linear kinetic equation can be solved analytically in the frame of Lagrangian droplet tracking schemes. The effect on the aerodynamic drag force on the droplet is taken into account by interpolation between the limiting geometries of spherical- and disc-shaped droplet. The model is widely used in CFD codes, however, the physical idealizations require fitting of several constants to empirical data. This introduces a certain problem-dependency and in many cases the model fails to describe important phenomena.

To study large distortions, Ibrahim et al. [7] present the Droplet Deformation and Breakup (DDB) model, which essentially is a nonlinear formulation of the TAB model equations. However, the necessity of time-resolved numerical integration seems not to be traded in for an essential improvement in physical accuracy. Thus, the DDB model has not found wide acceptance. Higher surface modes are taken into account by Normal Mode Analysis. The analysis has originally been devised by Rayleigh [13] as an exact theory for inviscid, small-amplitude shape oscillations of a free droplet. Lamb [10] suggested an extension to weakly dissipative fluids, Hinze [4] and Isshiki [8] later included the effect of an aerodynamic surface pressure distribution and successfully determined a geometrical criterion for the stability limit. Making use of this theoretical framework, Wiegand [17] formulates a quasi-steady model for the deformation-dependent aerodynamic drag force on a droplet. Other applications of Normal Mode Analysis for droplet deformation in gas flows have not been reported. Recently, Direct Numerical Simulation (DNS) of the internal and external flow fields accounting for the moving interface has been employed to study individual droplet deformation and breakup. However, due to the massive computational cost involved, these simulations are not suitable for direct use in spray computations.

The focus in the present paper is the coupled description of droplet propagation and droplet deformation including the onset of breakup. In particular the two-way coupling of both processes is accounted for by formulating a deformation dependent aerodynamic drag force and, on the other hand, using a differential description of the deformation process allowing for arbitrary variations in the relative flow conditions. The modeling framework is intended as a basis for a correlative description of the irreversible processes in the breakup phase [15], presented in combination in a future publication [14].

Normal Mode Analysis

The analysis is based on the fact, that any arbitrary droplet shape can be represented as a superposition of linearly independent surface eigenmodes, expressed mathematically as a series expansion in spherical harmonics. Considering axially symmetric deformation of a droplet in a uniform gas stream, the spherical harmonics are reduced to Legendre Polynomials $P_n(\cos\phi)$ [2] and the surface polar coordinate $r_s(t,\phi)$ is determined as follows

$$\frac{r_s}{R} = 1 + \sum_{n=0}^{\infty} \alpha_n P_n(\cos\phi) \, . \tag{2}$$

For small deviations from the spherical shape, exclusive pressure loading of the surface and interior potential flow, a matching polynomial expansion of the displacement field can be used to develop a series solution of the Navier-Stokes equations. The resulting second order differential equations describe the deformation kinetics in terms of the modal displacement functions $\alpha_n(t)$. The details of this analysis are reported in Hinze [4], Isshiki [8] or Schmehl [14]. In the present study, the equations derived by Isshiki—a straightforward extension of the Rayleigh-Lamb theory—are used in a non-dimensional representation on the time scale $T = t/t^*$

$$\frac{d^2\alpha_n}{dT^2} + 8(n-1)(2n+1)\frac{1}{\mathrm{Re}_{def}}\frac{d\alpha_n}{dT} + 8n(n-1)(n+2)\frac{1}{\mathrm{We}}\alpha_n = -2\,nC_n \, , \qquad n \geq 2 \, . \tag{3}$$

The equations show, that higher modes are increasingly suppressed and damped out so that only the first modes up to $n \approx 5$ significantly contribute to the deformation. The pressure boundary condition is contained in the expansion coefficients $C_n(t)$, which are defined as projections of the aerodynamic surface pressure distribution $p_s(t,\phi)$ onto the surface modes [2]

$$\frac{p_s - p_\infty}{\rho/2\, v_{rel}^2} = \sum_{n=0}^{\infty} C_n P_n(\cos\phi) \, , \qquad C_n = \frac{2n+1}{2}\int_0^{\pi} \frac{p_s - p_\infty}{\rho/2\, v_{rel}^2} P_n(\cos\phi)\sin\phi\, d\phi \, . \tag{4}$$

For small deformations, $p_s(t,\phi)$ can be approximated from the flow past a sphere which—assuming quasi-stationary behavior with respect to the deformation process—solely depends on the Reynolds number Re(t). Based on 46 individual pressure distributions retrieved from various sources in literature, discrete values of C_n have been computed (see Schmehl [14] for references). The result for the first 4 deformation modes is illustrated in Figure 1. To

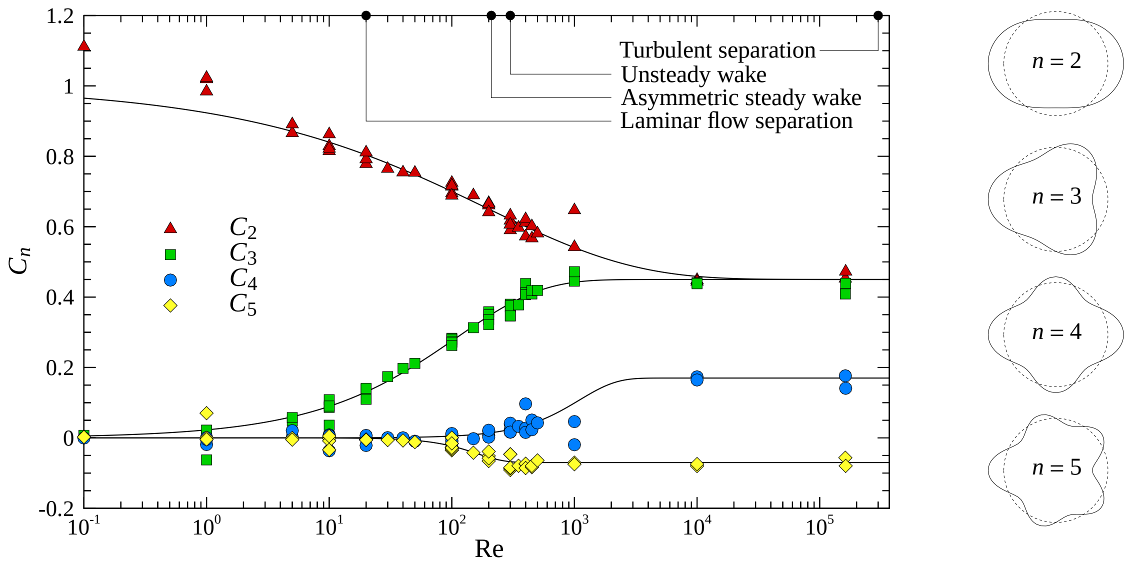

Figure 1: Expansion coefficients of pressure distributions on spheres (left), surface eigenmodes (right)

cover gradual variations of relative flow conditions during the deformation process, the following fitting functions have been developed

$$\begin{aligned} C_2 &= 0.45 + 0.55\,\exp(-0.15\,\mathrm{Re}^{0.36})\,,\\ C_3 &= 0.45 - 0.45\,\exp(-5.2\cdot10^{-2}\,\mathrm{Re}^{0.63})\,,\\ C_4 &= 0.17 - 0.17\,\exp(-3.9\cdot10^{-5}\,\mathrm{Re}^{1.45})\,,\\ C_5 &= -0.07 + 0.07\,\exp(-5.6\cdot10^{-5}\,\mathrm{Re}^{1.93}) \end{aligned} \tag{5}$$

These correlations are included in Figure 1 and map the complete sub-critical Reynold number range from Oseens solution ($C_2 = 1, \mathrm{Re} \to 0$) throughout Newtons regime of nearly constant c_D ($C_n \approx const., \mathrm{Re} \gtrsim 1000$). Assuming that shear forces on the droplet can be neglected, Equations 3 and 5 constitute a practically complete description of the linear problem, denoted in the following as Normal Mode (NM) model. Hinze [4] and Isshiki [8] introduce the concept of a critical stagnation point deformation $\alpha_c = \sum_n \alpha_n = -1$ reproducing well droplet breakup at steady and at sudden aerodynamic loading.

Nonlinear deformation modeling

At larger deformations the forces acting in and on the droplet are no longer independent of the state of deformation. Nonlinearities are further introduced by increased viscous stresses in the interior flow. Typical deviations from the linear behavior are mode coupling and shifting oscillation frequencies. Although basically feasible, mode expansion of the internal flow becomes computationally expensive, particularly in combination with the exterior problem of flow around a deformed droplet. Thus, as an alternative to mode expansion, the following concept is based on a presumed shape change via prolate and oblate spheroids. The basic configuration is illustrated in Figure 2. The displacement of the stagnation point and the radial equator coordinate are related by the general kinematic

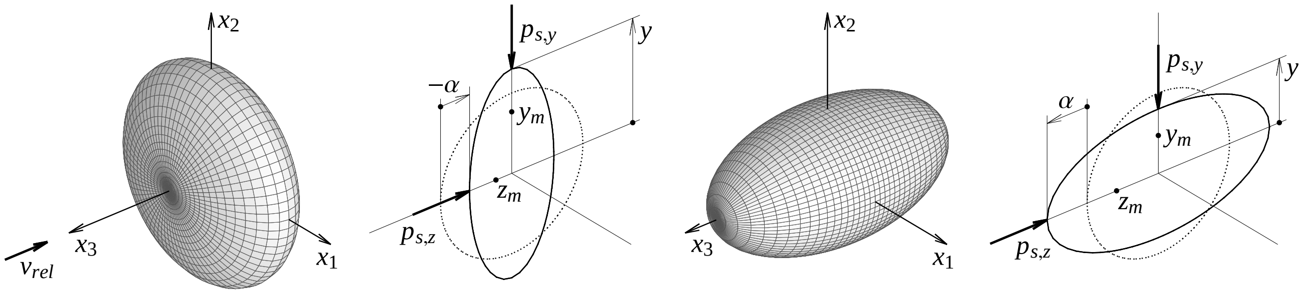

Figure 2: Reference frame and nondimensional geometry for oblate (left) and prolate spheroid (right)

condition $\alpha = 1/y^2 - 1$ which reduces to $\alpha = 2 - 2y$ in the linear limit $y \to 1$.

Starting point of the analysis is the balance of mechanical energy in the droplet-fixed reference frame

$$\frac{\rho_d}{2}\frac{d}{dt}\int_V v^2 dV + \sigma\frac{dS}{dt} = \int_S p_s v_n dS - \int_V \Phi_\mu dV \,. \tag{6}$$

Regarding the evaluation of the integral terms, it is important, that the resulting model equation asymptotically matches the linear theory underlying Equation 3 for the fundamental mode $n = 2$. Matching is enforced, if necessary, by introducing numerical correction factors.

For spheroids the rate of surface change can be calculated from exact analytical expressions for S. For the range of deformation considered, the following polynomials are used as an accurate and efficient approximation

$$\sigma\frac{dS}{dt} = \sigma\frac{dS}{dy}\frac{dy}{dt}\,, \qquad \text{with} \qquad \frac{1}{S_0}\frac{dS}{dy} = \begin{cases} 9.98y^3 - 30.34y^2 + 33.94y - 13.58\,, & 0.5 < y < 1\,, \\ 0.67y^3 - 4.01y^2 + 9.21y - 5.67\,, & 1 \le y < 2.3\,. \end{cases} \tag{7}$$

The kinetic energy of the deformation is described by the mass coordinates y_m and z_m characterizing radial (transverse) and axial mass movements in the droplet

$$y_m = \frac{1}{RV}\int_V \sqrt{x_1^2 + x_2^2}\,dV = \frac{3}{16}\pi y\,, \qquad z_m = \frac{1}{RV}\int_V \sqrt{x_3^2}\,dV = \frac{3}{8y^2}\,. \tag{8}$$

Suggesting a linear combination of the corresponding energy components, the rate of change can be formulated as

$$\frac{\rho_d}{2}\frac{d}{dt}\int_V v^2 dV = C_T\frac{\rho_d}{2}R^2 V\frac{d}{dt}\left[\left(\frac{dy_m}{dt}\right)^2 + \left(\frac{dz_m}{dt}\right)^2\right] = C_T\frac{3}{16}\pi\rho_d R^5\frac{dy}{dt}\left[\left(\frac{\pi^2}{4} + \frac{4}{y^6}\right)\frac{d^2y}{dt^2} - \frac{12}{y^7}\left(\frac{dy}{dt}\right)^2\right]. \tag{9}$$

The constant C_T enforces matching of nonlinear and linear formulations of the kinetic energy (the rate of energy change can not be matched due to the quadratic velocity term) at $y = 1$

$$C_T = \frac{512}{15\pi^2 + 240} \approx 1.32\,. \tag{10}$$

In a similar way, the work performed by the surface pressure is idealized by the surface point coordinates y and $z = 1/y^2$ characterizing the radial and axial movements of the surface. Assuming a cylindrical shape of the droplet defined by the corresponding normal surfaces $S_y = 4\pi R^2/y$ and $S_z = 2\pi R^2 y^2$ and using $p_{s,z} = \rho/2 v_{rel}^2$ and $p_{s,y} = -f p_{s,z}$ the rate of surface work can be approximated as

$$\int_S p_s v_n dS = C_W R\left[p_y S_y \frac{dy}{dt} + p_z S_z \frac{d}{dt}\left(\frac{1}{y^2}\right)\right] = -C_W \frac{\rho v_{rel}^2}{2} 4\pi R^3 (1+f)\frac{1}{y}\frac{dy}{dt} . \tag{11}$$

The factor $f > -1$ quantifies the external pressure drop along the surface. Matching Equation 11 to the linear theory is enforced by

$$C_W = \frac{2}{5(1+f)} C_2 , \tag{12}$$

formally substituting f by the parameter C_2. Although C_2 is specified exactly by projecting the surface pressure distribution to the surface mode $n = 2$ it is retained as an empirical parameter to fit the deformation response of the droplet to experimental data.

To calculate the rate of energy dissipation in the droplet, a characteristic value of the dissipation function

$$\Phi_\mu = 2\mu e_{ij} e_{ij} , \qquad \text{with} \quad e_{ij} = \frac{1}{2}\left(\frac{\partial v_i}{\partial x_j} + \frac{\partial v_j}{\partial x_i}\right), \tag{13}$$

has to be determined. Exploiting symmetries and continuity and further approximating the radial velocity gradient in the droplet (axis: $v_2 = 0$, equator: $v_2 = dy/dt$) gives

$$\int_V \Phi_\mu dV = 12\mu_d \int_V \left(\frac{\partial v_2}{\partial x_2}\right)^2 dV = 16\pi R^3 \mu \left(\frac{1}{y}\frac{dy}{dt}\right)^2 . \tag{14}$$

Recombining the idealized integral contributions, the energy balance of the droplet can be resolved on the time scale $T = t/t^*$ and leads to the following kinetic equation

$$\frac{\pi^2 + \frac{16}{y^6}}{\pi^2 + 16}\frac{d^2 y}{dT^2} - \frac{48}{\pi^2+16}\frac{1}{y^7}\left(\frac{dy}{dT}\right)^2 + \frac{40}{\mathrm{Re}_{def}}\frac{1}{y^2}\frac{dy}{dT} + \frac{20}{\mathrm{We}}\frac{1}{S_0}\frac{dS}{dy} = \frac{2C_2}{y} . \tag{15}$$

The normalized rate of surface change has to be substituted by the appropriate polynomial approximation given in Equation 7. To stress the formal similarity to the TAB model, Equation 15 is denoted as nonlinear TAB (NLTAB3) model. The version number 3 is retained for reference to Schmehl [14], where a detailed study of several model variants is performed. The linear equation of the TAB model can be derived from Equation 3 by setting $n = 2$ and $\alpha_2 = 2 - 2y$

$$\frac{d^2 y}{dT^2} + \frac{40}{\mathrm{Re}_{def}}\frac{dy}{dT} + \frac{64}{\mathrm{We}}(y-1) = 2C_2 \tag{16}$$

In the original formulation of the model O'Rourke and Amsden [11] suggest $C_2 = 2/3$, which corresponds well with values of C_2 from Figure 1.

Motion of deformed droplets

The effect of deformation on droplet motion can be significant. At maximum distortions typical for the stability limit, Hsiang and Faeth [6] report an increase of drag forces on the droplet by a factor of 4 for steady and 13 for shock loading. The experiments further reveal, that drag forces mainly scale with the cross sectional area and the degree of flattening of the droplet. Since this data is available from the models presented above, a geometry-based modeling concept is proposed for the aerodynamic drag force.

Assuming that aerodynamic force contributions can be either neglected or formally condensed into the steady state drag term, the droplets equation of motion is

$$m_d \frac{d\vec{u}_d}{dt} = \frac{\pi}{8} D^2 \rho\, c_D\, v_{rel}\, \vec{v}_{rel} + m_d \vec{g} . \tag{17}$$

In this equation, the effect of deformation is decomposed into the variation of the frontal area $\pi D^2 = \pi D_0^2 y^2$ of the droplet and the shape dependence of the drag coefficient c_D. Assessing various interpolation schemes for c_D, a linear scheme based on the quantity $f = 1 - E^2$ performs best in reproducing experimental drag data for spheroids (aspect ratio $E = 1/y^3$). Limiting geometries are the spherical shape ($E = 1$) and the disc shape ($E = 0$). To account for variable flow Reynolds numbers the following formulation is used

$$c_D = f\, c_{D,sphere} + (1-f)\, c_{D,disc}\,, \tag{18}$$

$$c_{D,sphere} = 0.36 + 5.48\,\mathrm{Re}^{-0.573} + \frac{24}{\mathrm{Re}}\,, \qquad \mathrm{Re} \lesssim 10^4\,, \tag{19}$$

$$c_{D,disk} = 1.1 + \frac{64}{\pi \mathrm{Re}}\,. \tag{20}$$

An alternative approach is proposed by Wiegand [17]. Avoiding a time-resolved description, he uses quasi-steady Normal Mode Analysis of droplet deformation to formulate an additive correction

$$c_{D,def} = \mathrm{We}\left(0.2319 - 0.1579\log\mathrm{Re} + 0.047\log^2\mathrm{Re} - 0.0042\log^3\mathrm{Re}\right) \tag{21}$$

of the standard drag coefficient $c_{D,sphere}$. For large accelerations unsteady aerodynamic forces on the droplet can be significant. At conditions typical for droplet breakup, these can be of the same order of magnitude as the steady forces. To approximate the effect, Temkin and Kim [16] suggest an additive, acceleration-dependent contribution to $c_{D,sphere}$.

Free shape oscillations

At low Weber numbers deformation by aerodynamic forces is less prominent. Yet, shape oscillations originating from other sources such as primary liquid breakup, droplet-droplet and droplet-wall collisions can still have a significant effect on the aerodynamic properties of the droplet—this is studied in the last section of this publication. The limiting case of free oscillations is particularly suitable to investigate the dynamic equilibrium of surface tension and momentum forces.

Small oscillations including weak viscosity effects are described by linear theory. For small values of We the time controlling the deformation process is shifting from t^* to $t^*_\sigma = (\rho_d D_0^3/\sigma)^{0.5}$. Transposing Equation 3 to the time scale $T = t/t^*_\sigma$ and solving this equation analytically leads to a non-dimensional damping constant $1/\tau = 20\,\mathrm{On}$ and an angular frequency $\omega^2 = 64 - 400\,\mathrm{On}$. In the inviscid case the latter reduces to $\omega_0 = 8$. For larger amplitudes or stronger viscosity effects the oscillation behavior increasingly deviates from linear theory. This effect is demonstrated by the parametric study illustrated in Figure 3. Further testing of several model variants reveals,

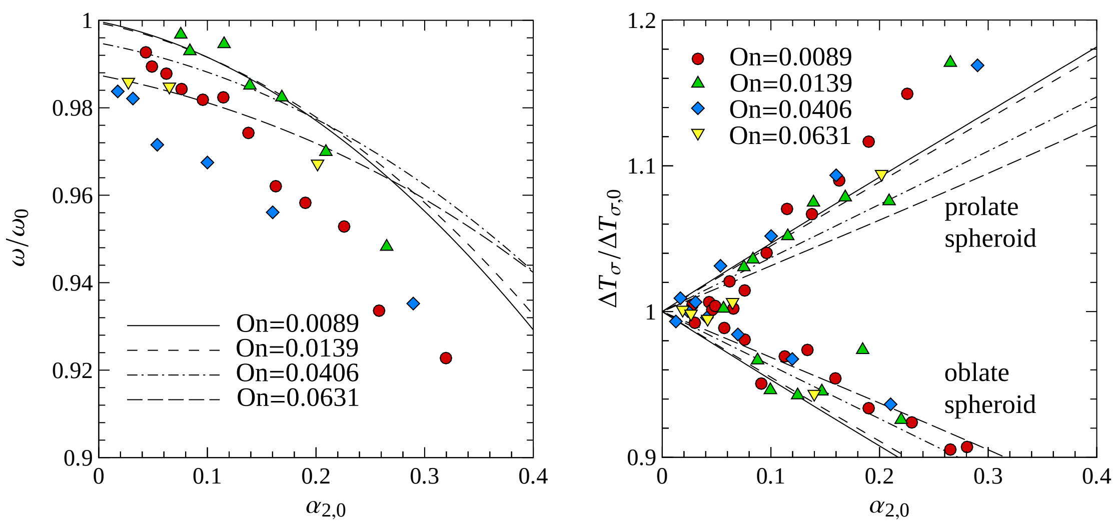

Figure 3: Shape oscillations in the fundamental mode: Frequency shift (left) and asymmetry of periods (right) normalized by $\omega_0 = 8$ and $\Delta T_{\sigma,0} = \pi/8$. Computations based on NLTAB3 model, experimental data from Kowalewski and Bruhn [9]

that only the simultaneous consideration of nonlinear surface tension and momentum forces, as realized in the NLTAB3 model, is able to reproduce the nonlinear characteristics. The decrease of ω/ω_0 for increasing values of On at small initial amplitudes $\alpha_{2,0}$ is a linear effect of viscous energy dissipation. According to $\omega^2 = 64 - 400\,\mathrm{On}$, a deviation of ω/ω_0 from 0.1% to 1% is attributed to an increase of On from 0.018 to 0.056. This range agrees well with the value of $\mathrm{On} = 0.024$ Kowalewski and Bruhn [9] suggest as a limit of linear theory. It further agrees with the onset of dissipation effects on shape oscillations in shock wave flows reported by Hsiang and Faeth [6].

Steady deformation in vertical gas flow

At We $\gtrsim 1$ deformation is increasingly governed by aerodynamic forces. For slow variations of relative flow conditions, the shape response of the droplet is quasi-steady. In the limiting case only surface tension and aerodynamic pressure forces affect the state of deformation (provided that the effect of shear stresses can be neglected). Demonstrating the ability of the NM model to reconstruct the shape of deformed droplets, computed static deformations are compared to photographies in Figure 4. It has to be noted, that only deformation is actually computed—relative

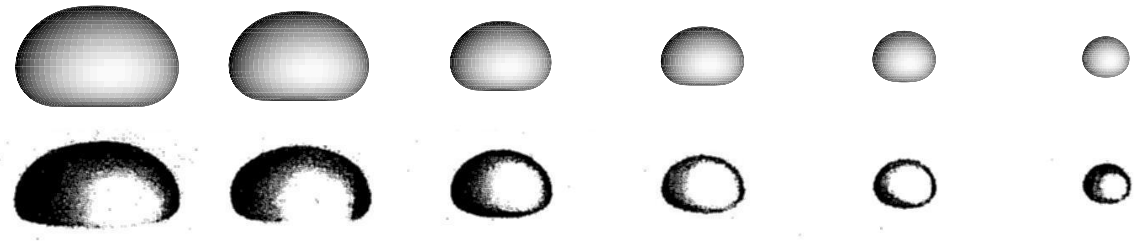

Figure 4: Droplets suspended in a vertical gas stream: Predictions based on the NM model (top) and experiment [12] (bottom). From left to right: $D_0\,[mm]$ = 8.00, 7.35, 5.80, 5.30, 3.45, 2.70 and v_{rel} = 9.20, 9.20, 9.17, 9.13, 8.46, 7.70 and We = 11.1, 10.2, 8.0, 7.3, 4.1, 2.6

flow conditions are prescribed by the measured values v_{rel} given in the caption. In spite of the underlying linear theory, shape computations and photographies agree rather well up to large distortions. In Figure 5 (left) the experimental data is compared to a parametric study of the various modeling approaches. In accordance to Figure

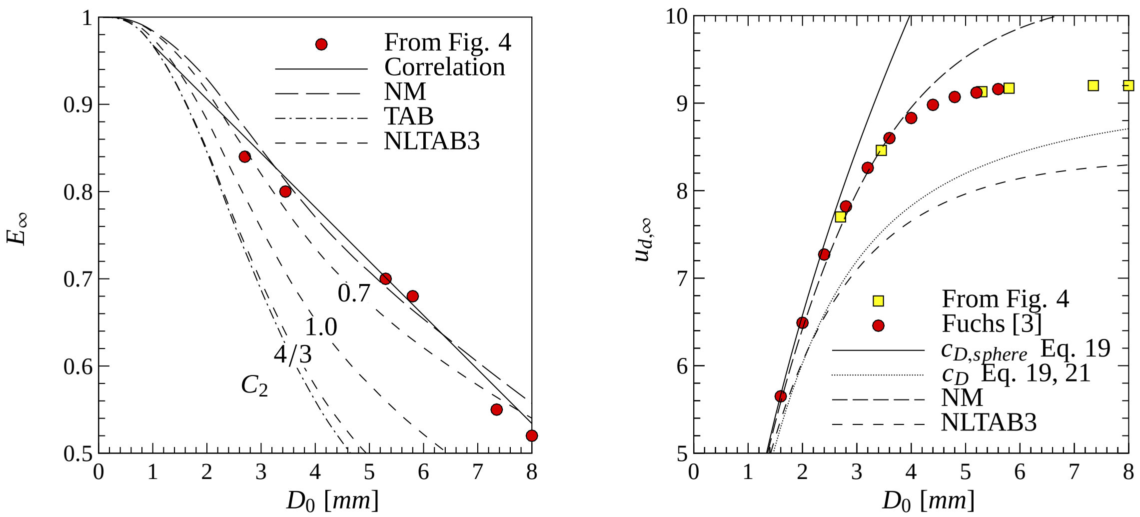

Figure 5: Steady deformation: v_{rel} prescribed (left) and computed from equation of motion (right)

4 the linear decrease of the aspect ratio suggested by Pruppacher and Beard [12] is well reproduced by the NM model. However, for small droplets computation and experiment deviate. Possible reasons are an effect of the neglected aerodynamic shear stresses (Re $\lesssim 1000$) or an accumulation of surface contaminants affecting surface tension. The influence of the model parameter C_2 is depicted for the NLTAB3 model. A value $C_2 = 2/3$, close to the theoretical value from normal mode expansion of $p_s(t,\phi)$ leads to deformations similar to the NM model. For values $C_2 > 0.7$ deformation is increasingly overestimated, in particular for larger droplets. The computations in Figure 5 (right) take into account simultaneous deformation and motion of the droplet. It is obvious, that the standard drag for a spherical droplet significantly underestimates the aerodynamic forces on a deformed droplet. The NM model is able to match the measured terminal velocities up to higher values of We, but fails to predict the asymptotic behavior for $D_0 > 6\ mm$. On the other hand, the quasi-steady deformation correction of c_D and the NLTAB3 model using $C_2 = 4/3$ both overestimate aerodynamic forces. For smaller values of C_2 the computed values of $u_{d,\infty}$ approach the experimental data. Thus, regarding steady state deformation of a droplet a value of $C_2 = 2/3$ is recommended.

Deformation in shock wave flow

A sudden increase in relative flow velocity results in a dynamic shape response of the droplet. The phenomenon is of particular importance in many multiphase flow applications including air-assisted atomization. Figure 6 illustrates the dynamic response by a sequence of computed droplet shapes. As a basic rule from linear theory,

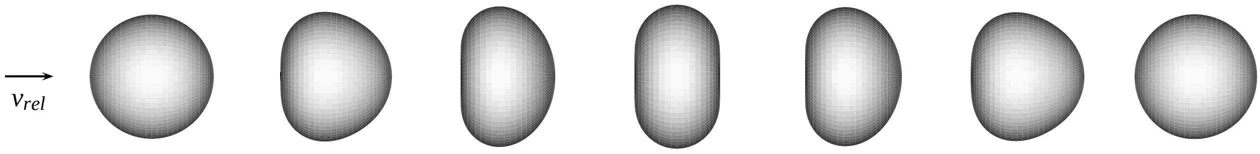

Figure 6: Computed shape response to sudden aerodynamic loading with $\mathrm{We} = 5, \mathrm{Re}_{def} = 666$ and $\mathrm{Re} = 1100$ in time steps of $\Delta T = 0.3$ using the NM model.

maximum deformations from sudden loading are approximately twice as large as the steady values at the same Weber number (overshoot effect [6]). A quantitative study of maximum transverse distortions is presented in Figure 7 (left). Droplet motion is not included in these computations—a realistic assumption since the time scale

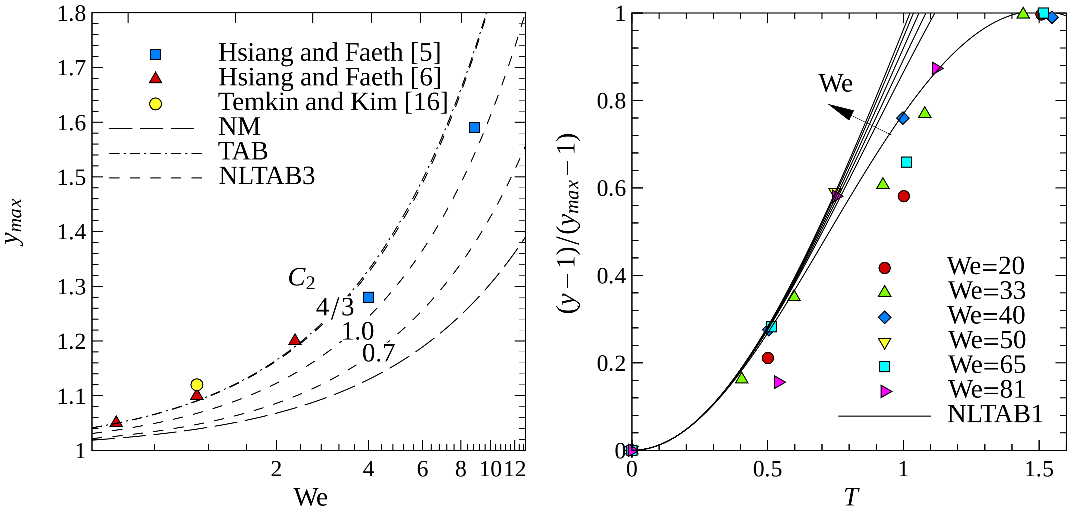

Figure 7: Maximum transverse distortions at sub-critical conditions (left), initial dynamic response prior to droplet breakup, experimental data from Dai and Faeth [1] (right)

of droplet acceleration in shock wave flows is generally larger than the characteristic time of the initial flattening of the droplet. Most noticeable is a substantial underestimation of the maximum deformation by the NM model and the NLTAB3 model for $C_2 = 2/3$. However, matching can be enforced by increasing C_2. At $\mathrm{We} \sim 1$ a value of $C_2 = 4/3$ achieves best agreement with the data. To reproduce the critical transverse distortion $y_{max} = 1.8$ of the droplet observed in experiments at $We_c = 13$ [6, 1], Figure 7 suggests a value of $C_2 = 1$.

A possible reason for the underestimation of distortion by the steady value of C_2 is an additional effect of unsteady forces on the droplet surface. The effect, which is associated with the significant increase of the aerodynamic drag force on accelerated droplets [16] is not considered in the present modeling concepts. Comparing the TAB and NLTAB3 models indicates, that nonlinear effects have only minor influence on maximum distortions.

Regarding droplet breakup at $We > We_c$, Figure 7 (right) illustrates the temporal evolution of the initial flattening of the droplet. Agreement of experiment and computations is satisfactory and the data shows only a minor influence of We on the velocity of flattening when normalized by the maximum deformation.

Deformation and deflection in horizontal nozzle flow

Finally, deformation and deflection of water droplets falling in the horizontal jet from a nozzle is studied. The experimental configuration is explained in detail in Wiegand [17]. Chosen here is his case 17-3W, which is characterized by a high sub-critical Weber number $\mathrm{We}_0 = 11.8$ at atmospheric laminar flow conditions. Other initial values and boundary conditions are given by $Re_0 = 2414$, $D_0 = 0.546\ mm$, $u_x = 36.6\ m/s$, $u_{d,x,0} = 0.663\ m/s$ and

$u_{d,y,0} = -4.76\ m/s$. The NLTAB3 model is applied with $C_2 = 4/3$. The experimental data and the results are illustrated in Figure 8. As a consequence of the generation process the droplets enter the nozzle flow with significant

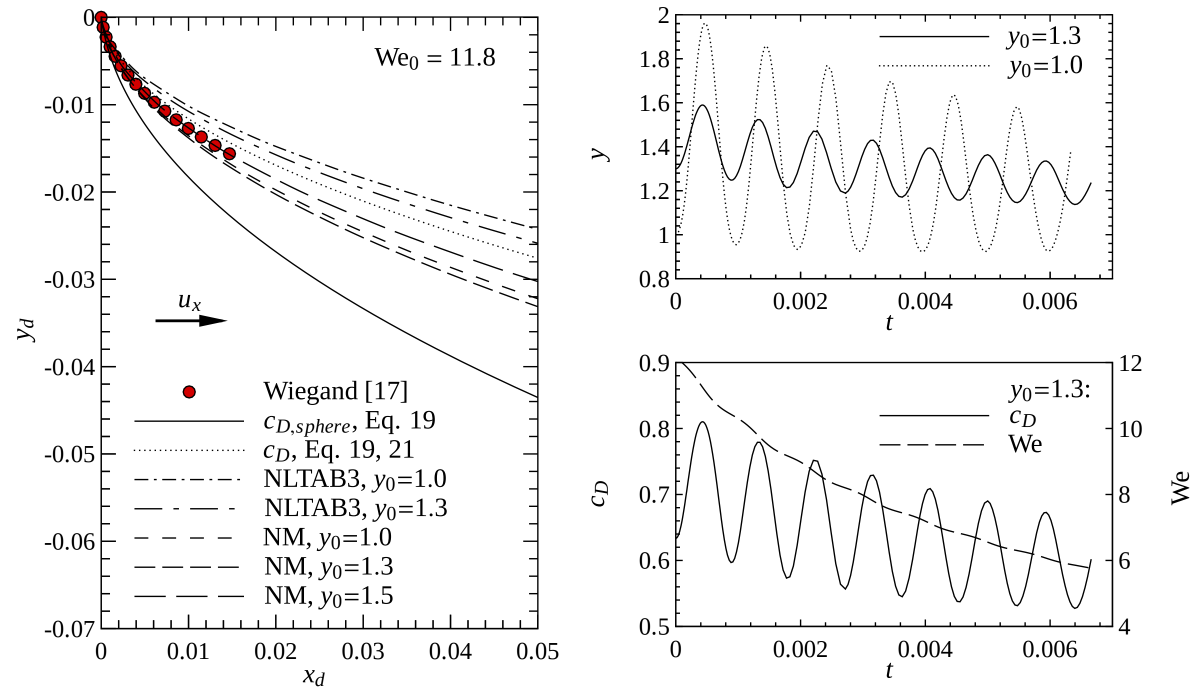

Figure 8: Droplet trajectories deflected in horizontal nozzle flow (left) and trajectory data computed with the NLTAB3 model (right)

shape oscillations. To demonstrate the influence of these oscillations, trajectories of droplets with different initial deformations y_0 are depicted.

Conclusions

Two different concepts have been developed for the numerical simulation of droplet deformation and breakup by aerodynamic pressure forces. The NM model is feasible of resolving complex shape dynamics. It is based on linear Normal Mode Analysis combined with correlations for the pressure boundary condition on the droplet surface. The NLTAB3 model presumes a deformation of the droplet into prolate and oblate spheroids and incorporates nonlinear force effects at larger deformations. Both concepts account for modification of the aerodynamic drag forces by deformation and have been evaluated for multiphase flow scenarios typical for mixture preparation processes. The computations show, that for $\mathrm{We} \gtrsim 1$ deformation by aerodynamic forces has an essential effect on droplet motion and, on the other hand, droplet motion in the flow field affects the deformation process by changing local flow conditions. For certain cases a quasi-steady formulation of a We-dependent drag coefficient can be sufficient to reproduce average droplet trajectories. However, even at low We, shape oscillations can arise from initial distortions influencing the aerodynamic properties of the droplet. It is evident, that the effect of aerodynamic forces can deviate substantially from the effect of a steady surface pressure distribution assumed in the modeling concepts. Particularly at high droplet accelerations maximum distortions are underestimated. Although this can be corrected empirically by adapting model parameters, further research should be conducted on the nature and effect of aerodynamic forces.

Acknowledgments

The author would like to thank Herbert Wiegand for contributing valuable experimental material.

References

[1] Z. Dai and G. M. Faeth. Temporal Properties of Secondary Drop Breakup in the Multimode Breakup Regime. *International Journal of Multiphase Flow*, 27(2):217–236, 2001.

[2] H. F. Davis. *Fourier Series and Orthogonal Functions*. Dover Publications, 1989.

[3] N. A. Fuchs. *The Mechanics of Aerosols*. Pergamon Press, Oxford, 1964.

[4] J. O. Hinze. Forced Deformations of Viscous Liquid Globules. *Applied Scientific Research*, A1:263–272, 1948.

[5] L.-P. Hsiang and G. M. Faeth. Near-Limit Drop Deformation and Secondary Breakup. *International Journal of Multiphase Flow*, 18(5):635–652, 1992.

[6] L.-P. Hsiang and G. M. Faeth. Drop Deformation and Breakup Due to Shock Wave and Steady Disturbances. *International Journal of Multiphase Flow*, 21(4):545–560, 1995.

[7] E. A. Ibrahim, H. Q. Yang, and A. J. Przekwas. Modeling of Spray Droplets Deformation and Breakup. *AIAA–Journal of Propulsion and Power*, 9:651–654, 1993.

[8] N. Isshiki. Theoretical and Experimental Study on Atomization of Liquid Drop in High Speed Gas Stream. Technical Report 35, Transportation Technical Research Institute, 1959.

[9] T. A. Kowalewski and D. Bruhn. Nonlinear Oscillations of Viscous Droplets. In IPPT PAN Warszawa 1994 Akiyama, Kleiber, editor, *Proc. of Japanese-Centr. European Workshop on Adv. Comp. in Eng., Pultusk*, pages 63–68, 1994.

[10] H. Lamb. *Hydrodynamics*. Cambridge at the University Press, 6 edition, 1932.

[11] P. J. O'Rourke and A. A. Amsden. The TAB Method for Numerical Calculation of Spray Droplet Breakup. *SAE 872089*, 1987.

[12] H. R. Pruppacher and K. V. Beard. A Wind Tunnel Investigation of the Internal Circulation of Water Drops Falling at Terminal Velocity in Air. *Quarterly Journal of the Royal Meteorological Society*, 96:247–256, 1970.

[13] Lord Rayleigh. *The Theory of Sound*, volume 1. Reprinted 1945 by Dover, 1877.

[14] R. Schmehl. Tropfendeformation und Nachzerfall bei der Gemischaufbeitung in Verbrennungskraftmaschinen. Dissertation, Institut für Thermische Strömungsmaschinen, Universität Karlsruhe (TH), in preparation. Will be available from http://www.its.uni-karlsruhe.de/~schmehl.

[15] R. Schmehl, G. Maier, and S. Wittig. CFD Analysis of Fuel Atomization, Secondary Droplet Breakup and Spray Dispersion in the Premix Duct of a LPP Combustor. In *8th International Conference on Liquid Atomization and Spray Systems, ICLASS 2000, Pasadena, USA*, 2000.

[16] S. Temkin and S. S. Kim. Droplet Motion Induced by Weak Shock Waves. *Journal of Fluid Mechanics*, 96: 133–157, 1980.

[17] H. Wiegand. Die Einwirkung eines ebenen Strömungsfeldes auf frei bewegliche Tropfen und ihren Widerstandsbeiwert im Reynoldszahlenbereich von 50 bis 2000. *Fortschrittberichte VDI*, Reihe 7, Nr. 120, 1987.

[18] A. Wierzba. Deformation and Breakup of Liquid Drops in a Gas Stream at nearly Critical Weber Number. *Experiments in Fluids*, 9:59–64, 1990.